

# Substantiation of Parameters for Long-Term Strength Testing of Materials

R.A.Hasanov<sup>1</sup>, A.M.Babaev<sup>2</sup>, M.I.Kazimov<sup>3</sup>, G.S.Cheyrabadi<sup>4</sup>, S.A.Musavi<sup>5</sup>, T.M.Gasimova<sup>6</sup>,  
F.Ch.Ramazanov<sup>7</sup>, A.I.Zeynalov<sup>8</sup>, T.R.Karimova<sup>9</sup>

Professor, Department of Mechanics, Azerbaijan State Oil and Industry University, Baku, Azerbaijan<sup>1</sup>

Ph.D., Student, Department of Mechanics, Azerbaijan State Oil and Industry University, Baku, Azerbaijan<sup>2,5-9</sup>

Ass. of Professor, Department of Mechanics, Azerbaijan State Oil and Industry University, Baku, Azerbaijan<sup>3,4</sup>

**Abstract:** Austenitic stainless steel (German and USA (AISI) designations respectively X2CrNiMo18-14-3 and 316L) was studied in stress controlled tests on the high cycle fatigue (HCF) regime in air at room temperature. Stress-strain responses were carefully measured to clarify the stress amplitude dependent fatigue behaviour of this steel. The fatigue tests were performed at constant-amplitude cyclic loading with load ratio of  $R = -1$ . Results showed that the fatigue limit of AISI 316L stainless steel at room temperature was 190-200 MPa.

**Keywords:** Fatigue strength, stainless steel, HCF.

## I. INTRODUCTION

The technical challenges for the oil and gas industry e.g. increased depths, tar sands, heavy oils, sourer medium, arctic and high pressure and temperature conditions require materials able to cope with these harsh environments. Austenitic stainless steels due to corrosion resistance, excellent mechanical properties tends to replace traditional carbon steel. Oil and gas platforms regularly use stainless steel tubing in process instrumentation, as well as in chemical inhibition, hydraulic and utility applications, over a wide range of temperatures, flows, and pressures, widely used as the sealing materials (Ring Type Joints etc.) where high pressure/temperature applications necessitated the need for a high integrity seal.

One of the most frequent causes of failure in materials, including stainless steels using in the oil and gas equipment, is fatigue failure. The cyclic nature of operation causes many changes in material behavior leading to failures of components (turbine blades, engine parts, oil/gas pipes) to be subjected to both cyclic straining and continuous deformation. Cyclic fatigue is caused by repeated fluctuating loads and initiates small (micro) cracks in the material and causes them to grow into large (macro) cracks due to change its mechanical properties on the exploration process. The fatigue strength for austenitic stainless steels are related to the yield and tensile strength levels [1].

Table 1. Chemical compositions of AISI 316L

Steel designation		Component % by mass								
		C	Si	Mn	P	S	N	Cr	Mo	Ni
European	X2CrNiMo18-14-3	≤0.030	≤1.00	≤2.00	≤0.04 5	≤0.01 5	≤0.11	17.0 to 19.0	2.50 to 3.00	12.5 to 15
German	1.4435									
USA (AISI)	316L									
ГОСТ 5632-72	03KH17N14M3									

## II. EXPERIMENTAL STUDY

### 1. MATERIAL OF SPECIMENS

Austenitic stainless steel AISI 316L used in the specimens' fabrication. These steels are more ductile than carbon grades which manifests as an ability to achieve large plastic strains in the range between yield strength and ultimate tensile strength. Performed tensile test of the specimens from the same material on the ZWICK Tensile machine to identify mechanical properties are shown at Table 2.

Table 2. Mechanical Properties of Type 316L Stainless Steel

Mechanical Properties	316L
Yield Point, MPa	340
Ultimate (U.T.S.) Tensile strength, MPa	560
Modulus of Elasticity, GPa	193
Elongation at break, %	45.0
Hardness, max BHN	217

Table 3 shows mechanical properties for the different types of austenitic stainless steels 316L [2] minimum required properties in the annealed condition at room temperature.

Table 3 Mechanical properties of stainless steels in the annealed condition at room temperature

Type of stainless steel	Grade of steel	Hardness HB, max	0.2% proof strength $R_{p0.2}$ , [MPa], min	Tensile strength $R_m$ , [MPa]	Elongation after fracture A [%], (long.)
Austenitic	1.4435 (AISI316L)	215	200	500-700	40

The increase of yield strength and tensile strength (Table 1) of austenitic stainless steels is related to their high content of carbon (C) and nitrogen (N) which are alloying elements that improve these properties.

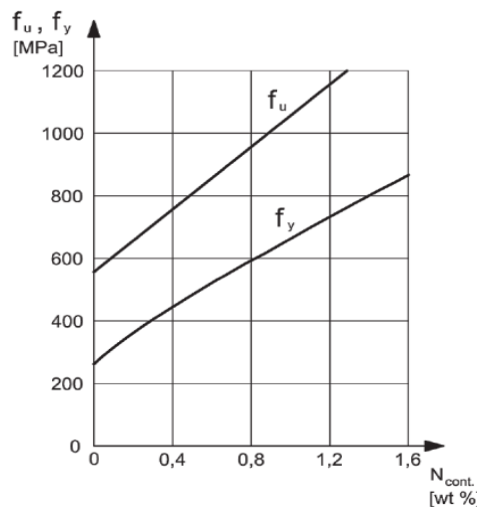


Figure 1. Effect of nitrogen on the strength of austenitic stainless steels [2, 3]: where  $f_u$  – ultimate tensile strength,  $f_y$  – yield strength

If the nitrogen (N) content is increased from 0.05% to 0.20%, an increase of yield strength from 270MPa to 340MPa will be achieved [3]. Figure 1 shows the influence of nitrogen (N) content on yield strength (0.2% proof strength  $R_{p0.2}$ ) and ultimate tensile strength of austenitic steels.

## 2. DESIGN OF SPECIMENS

Experiments conducted for the fatigue testing of cylindrical unnotched specimens subjected to constant amplitude ( $R = -1$ , i.e. fully reversed) in HCF regime, where the strains are predominately elastic, in air at room temperature and laboratory air/humidity environment.

Specimens were designed as per ASTM E466 [4]. Dimensions of the specimens with tangentially blended fillets between the test section and the ends are given in the Fig. 2:

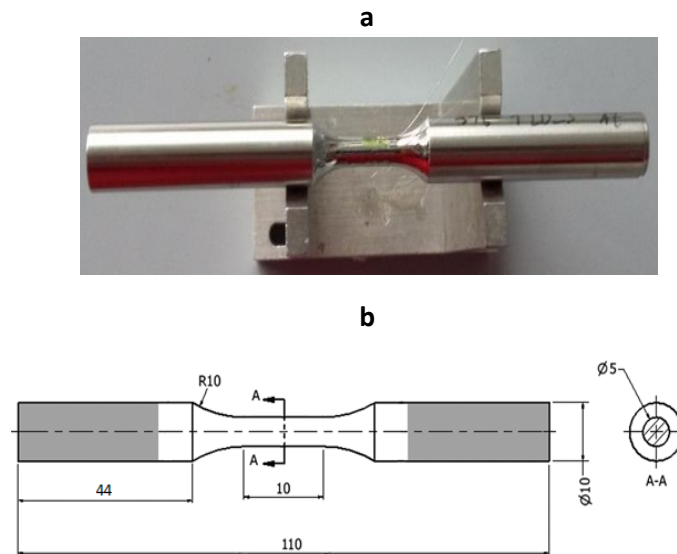


Figure 2. Specimen’s dimensions in mm (b) and electropolished test surface with strain gauge (a)

Grip cross-sectional area diameter is  $\text{Ø}10$  mm, 2.0 times of the test section area. The blending fillet radius is  $r10$  mm, to minimize the theoretical stress concentration factor of the specimen. The gauge length is  $L10$ mm and approximately two times of the test section diameter (to minimize buckling during reverse run in compression). The diameter of the test section is at least  $\text{Ø}5.00$  mm. The design of the specimen set so that failure occurs in the test section (reduced area as shown in Fig. 2a). The surface of gauge section was electropolished. Electropolishing is commonly applied to the preparation of metal samples because this process doesn’t cause mechanical deformation of surface layers usually observed when mechanical polishing is used.

### 3. HCF TESTS ON THE RESONANCE-TESTING MACHINE

The fatigue test procedure carried out in accordance with the American Society for Testing and Materials (ASTM) E466, “Conducting Constant Amplitude Axial Fatigue Tests of Metallic Materials”.

Resonance testing systems may be divided into two general groups: (1) sub-resonant systems that operate just below the resonant frequency of the specimen-machine system (that is, on the rising slope of the force amplitude-frequency curve, Point A, Fig. 4b) and (2) resonant machines which operates at the resonant frequency of the specimen-machine system (that is, at the top of the force amplitude-frequency curve, Point B, Fig.4b). Operating at sub-resonance may be achieved by holding the mass of moving elements constant and regulating the speed. It may be seen in Fig. 4b that slight fluctuations in speed at frequencies well away from the resonant frequency cause only small variations in load amplitude. However, similar variations in operating speed at frequencies near resonance can cause significant variations in load amplitude. It is desirable in the latter case to tune the system by varying the mass of the moving elements rather than varying the driving frequency. Another cause of load fluctuation is the change in resonance frequency of the system due to a decrease in specimen stiffness as the cracks appears and grows.

Experiments for the HCF performed on the Resonance-testing-machine TESTRONIC by RUMUL (Figure 3).

Table 3. RUMUL resonant fatigue machine parameters

Nominal load, kN	Max. static load, kN	Max. dynamic load, kN	Frequency range, Hz	Daylight between columns, mm	Frequency steps <sup>1</sup>	Max. vertical space, mm	Total height, mm	Total weight, kg
250	250	± 125	40 - 260	500	8	600	2700	3000

<sup>1</sup> The operating frequency depends on the stiffness of the specimen

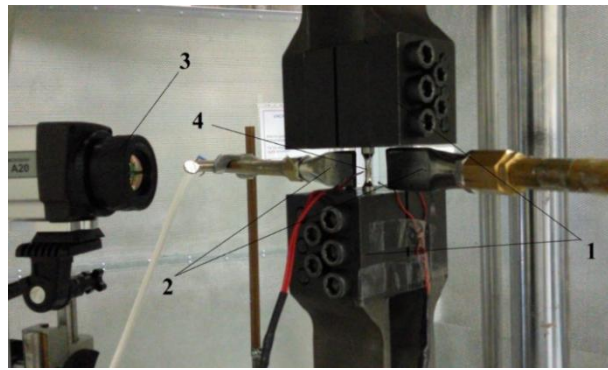


Figure 3. Main view of test bench: 1- clamps; 2 – compressed air supplies for the specimen cooling; 3 – infrared camera for the temperature measurement; 4 – specimen with strain gauge. This testing-machine is designed for forces up to 250 kN and displacements up to 8 mm. The realizable frequency ranges from 45 to about 260 Hz (Table 3).

In this test-machine during loading process specimen serves as a spring element between two mutually resonating masses (Fig. 4). The spring-mass system is excited by an electromagnet to a sinusoidal vibration. By simplification of the clamping system and the specimen with a gauge length  $L$ , the cross-sectional area  $A_F$  and the modulus of elasticity  $E$ , the natural frequency  $f_0$  can be connected by the equation:

$$f_0 = \frac{1}{2\pi} \sqrt{\frac{EA_F}{L} \frac{m_0 + m_1}{m_0 \cdot m_1}}$$

where:  $m_0$  and  $m_1$  – weight of the oscillating mass,  $E$  – elastic modulus of specimen material,  $f_0$  natural frequency of the system.

The dynamic load is generated by a maintenance free oscillating system (resonator). The oscillating system consists of masses and springs, the specimen itself being part of this oscillating system. RUMUL resonant testing machines work at full resonance, i.e. the operating point is situated on the top of the resonance curve, achieving thus a very high amplification of the applied excitation load (Fig.4b, Point B).

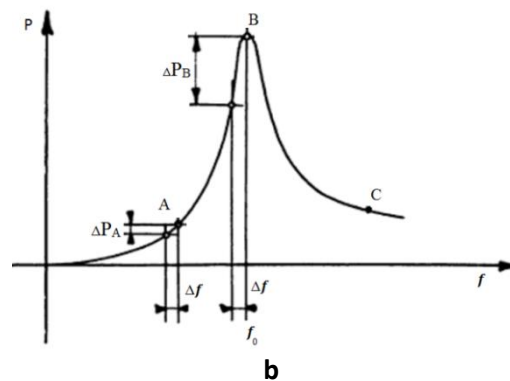
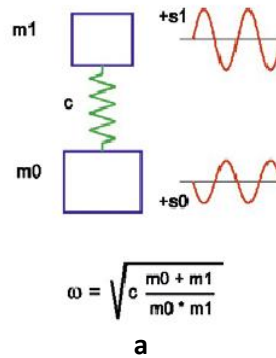


Figure 4. Two-Mass-Oscillating-System (simplified) (a) and resonance curve of a resonance fatigue testing machine (b) Machine itself is tuned to a different frequency corresponding to the natural frequency of the specimens when changing of its natural frequency (by varying of the specimens' geometry  $A_F$ ,  $L$ ). In case of RUMUL TESTRONIC resonant-testing-machine, machine completed fatigue tests either since it identifies significant changes in resonance frequency (by keeping of weight of oscillating mass constant), which happens due to decrease of specimens' stiffness or the

fatigue cycles reached  $10^7$  cycles. While machine detects frequency drop (generated by a fatigue crack), stops test, however these cracks cannot be visible by naked eyes (Fig. 5). In order to measure the specimens' temperature evolution faithfully, a non-destructive evaluation method, thermography, was utilized infrared (IR) thermography for the temperature.

Due to the specimen geometry, the stress was concentrated at the specimen-gage section, and the heat generated in the material was mainly conducted through the axial direction of the specimen. Hence, the highest temperature was always located at the midpoint of the surface of the specimen-gage section. Fortunately, in the HCF regime, the plasticity is often minuscule so that specimen heating, while ever present, does not restrict testing [5].



Figure 5. Cracks induced machine to stop experiment; specimen D10 at stress amplitude 230 MPa

Several specimens (Figure 2b) (10-13 items) were tested and S-N diagram, constant cyclic stress amplitude  $\sigma_a$  is applied and number of cycles to failure ( $N_f$ ) of specimens were determined. Loading frequency was varying between 100-120 Hz.

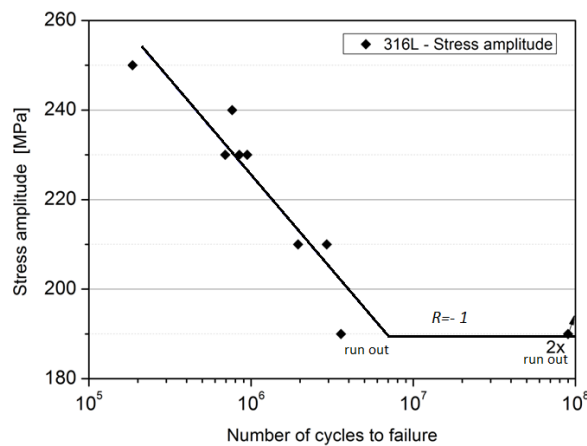
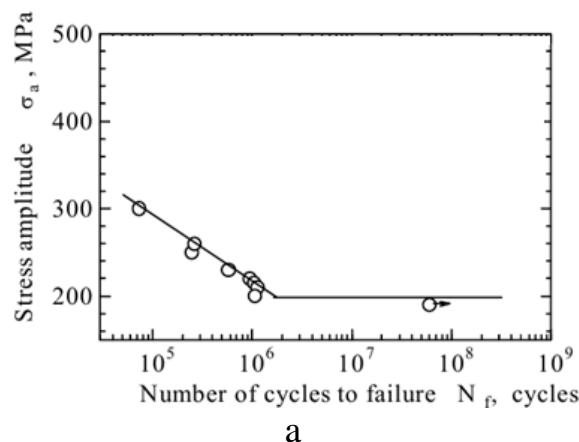
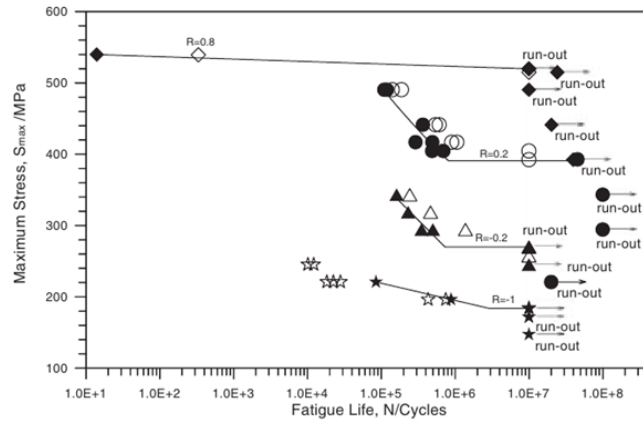


Figure 6.  $S - N$  (Wöler) diagramm -  $\sigma_a - \log(N_f)$

Using  $S - N$  curve (Fig. 6) can be identified the stress endurance limit  $\sigma_e = 190 - 200 \text{ MPa}$  (fatigue strength) below which present specimens don't cause failure.

Figure 7 shows the  $S - N$  curves for specimens tested under different stress amplitudes ( $R = -1$ ) at room temperature by different researchers. Test result in Fig. 7a is from rotating bending fatigue tests at 50Hz under water-cooling condition by deionized water [6]. The results of the fatigue tests are shown in Figure 7b, are for specimens in various stress amplitudes at RT and 20 Hz in axial loading [7]. The fatigue limit of this AISI 316L specimens is about 190-200 MPa.





b

Figure 7. (a) Rotating bending tests at 50 Hz under water-cooling condition by deionized water, (b) axial loading tests of specimens in various stress amplitudes at RT and 20 Hz

It should be noted that there are several shortcomings of  $S - N$  fatigue data. First, the conditions of the test specimens do not always represent actual service conditions which differs from the condition of the test specimens will have significantly different fatigue performance. Furthermore, there is often a considerable amount of scatter in fatigue data even when carefully machined standard specimens out of the same lot of material are used. Since there is considerable scatter in the data, a reduction factor is often applied to the  $S - N$  curves to provide conservative values for the design of components [7].

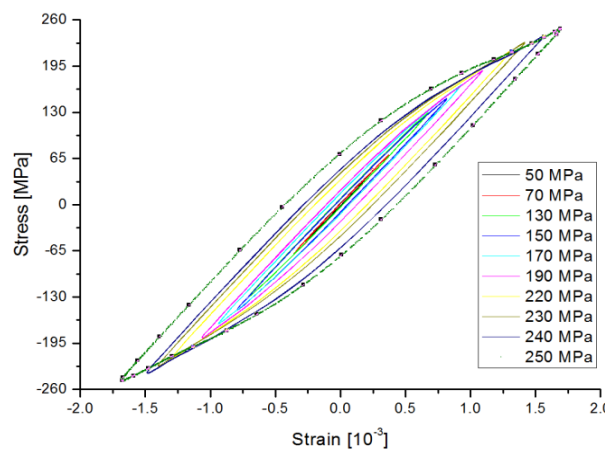


Figure 8. Schematics of a small hysteresis loops produced in various stress amplitudes

In the high cycle fatigue regime, the stress amplitude  $\sigma_a$  is typically below the cyclic yield strength,  $\sigma_{0.2}$ , of the material, and this produces small stabilized hysteresis loops, Figure 8.

HCF - High cyclic fatigue can occur in the elastic range of deformation, the body from ductile material is destroyed without distortion of shape and dimensional changes. The area within the loop is the energy per unit volume dissipated as plastic work during a cycle. In the high cycle regime, this energy dissipation (loss) is small, and it decreases rapidly as the stress amplitude decreases. However, if the imposed stress amplitude increases beyond the cyclic yield strength  $\sigma_{0.2}$ , then the cyclic plastic strain amplitude and the width of the stabilized hysteresis loops rapidly become large, and the resulting fatigue life typically decreases to below  $\approx 10^4$  cycles (LCF) [8].

### CONCLUSION

Several tests were carried out at room temperature to identify the endurance limit of austenitic 316L stainless steel. The factors of cost and time limitations are among the reasons that fatigue tests were to be performed in resonant fatigue machine. The fatigue tests of the experiment recorded that the fatigue limit for AISI 316L austenitic steels is 190 MPa. During cyclic loading, AISI 316L exhibits rapid hardening during the first 50–100 cycles; the extent of hardening increases with increasing stress amplitude and decreasing temperature and strain rate. Crystallographic observation of the samples prepared from specimens subjected to cyclic loadings at various stress amplitudes will be performed on the TEM/SEM microscopes.

**ACKNOWLEDGMENT**

This material is based upon work supported by the German Academic Exchange Service (DAAD) research foundation at the Department of Materials Science and Materials Testing of the Siegen University (Germany) in 2015.

**REFERENCES**

- [1] Life time prediction using accelerated test data of the specimens from mechanical element, Zaharia, S.M., Martinescu, I., Morariu, C.O., *Eksplotacja i Niezawodnosć – Maintenance and Reliability*, 14 (2012) 99-106.
- [2] EN 10088-5:2009. Stainless steels – Part 5: Technical delivery conditions for bars, rods, wire, sections and bright products of corrosion resisting steels for construction purposes.
- [3] International Molybdenum Association, Practical guidelines for the fabrication of high performance austenitic stainless steels, London 2010.
- [4] ASTM E466-Standard Practice for Conducting Force Controlled Constant Amplitude Axial Fatigue Tests of Metals
- [5] *Fatigue and Durability of Structural Materials*, S. S. Manson, G. R. Halford, 2006 ASM International
- [6] Estimation of high cycle fatigue limit of hard shot peened austenitic stainless steel, K. Masaki, Y. Ochi and T. Matsumura, Department of Mechanical Engineering and Intelligent Systems, The University of Electro Communications Tokyo, 1-5-1, Chofugaoka, Chofu, Tokyo, 182-8585, Japan;
- [7] High-Cycle Fatigue Behavior of Type 316L Stainless Steel, Jiunn-Yuan Huang\*, Ji-Jung Yeh, Sheng-Long Jeng, Charn-Ying Chen and Roang-Ching Kuo - *Materials Transactions*, Vol. 47, No. 2 (2006) pp. 409 to 417, 2006 The Japan Institute of Metals;
- [8] Estimation of High Cycle Fatigue limit of hard shot peened austenitic stainless steel, K. Masaki, Y. Ochi and T. Matsumura, Department of Mechanical Engineering and Intelligent Systems, The University of Electro Communications Tokyo, 1-5-1, Chofugaoka, Chofu, Tokyo, 182-8585, Japan.